Temperature-Variable Characteristics and Noise in Metal–Semiconductor Junctions

ERIK L. KOLLBERG, SENIOR MEMBER, IEEE, HERBERT ZIRATH, AND ANDRZEJ JELENSKI, MEMBER, IEEE

Abstract — **Although metal–semiconductor junctions were first explored a hundred years ago, some important aspects of the transport mechanism of electrons across the metal–semiconductor barrier have not yet been fully explained. In this paper, we report on a new model and supporting experimental results which explain deviations observed from the ideal exponential current–voltage characteristic. The model and results are applicable to the optimization of microwave and millimeter-wave front ends.**

I. Introduction

In recent years, low-noise millimeter-wave mixers have been constructed using cryogenically cooled Schottky-barrier diodes with small junction capacitances [1]–[3]. Major advances occured after the importance of appropriate matching networks was recognized and optimized embedding networks had been developed [4], [5]. However, a number of physical mechanisms which affect the nonlinear properties and the noise of the diode were not understood. Thus, the construction of an optimized front end remained an art because a sufficiently accurate model of the junction had not been found [7]–[9].

The purpose of this paper is to report on measurements performed on GaAs Schottky diodes fabricated at AT&T Bell Laboratories and other research laboratories and to develop transport models which are consistent with our experimental results. The measurements include temperature-variable current–voltage characteristics and microwave noise generated as a function of dc current. The obtained results depend directly upon the geometry and physical properties of the junction and are independent of the complexity of embedding networks and the generation of multiple spurious mixing products.

II. Basic Experiment Results

Noise and log $I(V)$ characteristics of a number of GaAs Schottky-barrier diodes manufactured in several laboratories were measured. The typical diode geometry is shown in Fig. 1 and basic data for some investigated diodes are given in Table I. An example of log $I(V)$ characteristics measured in the 20–300-K temperature range are shown in Fig. 2. It was found for measured diodes, particularly at low temperatures, that it was impossible to assign to a log $I(V)$ curve a single slope parameter. As shown in Fig. 2, each curve seems to be composed of 3–4 segments with different slopes.

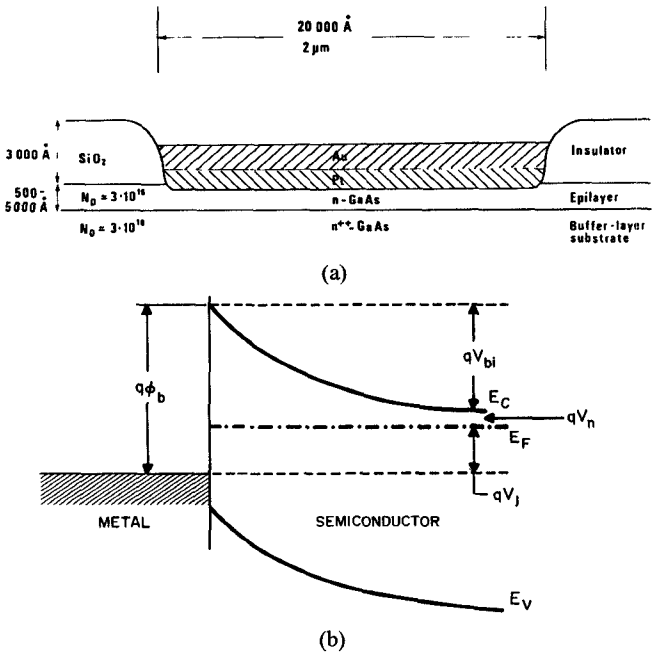

Fig. 1. (a) Cross-sectional view of a typical millimeter-wave Schottky-barrier diode. (b) Energy-band diagram of a metal–semiconductor junction.

Values for the diode series resistance R_s given in Table II (measured) were obtained by an algorithm assuming that the current–voltage characteristic of the barrier was exponential, and R_s constant. However, real diodes show deviations from this ideal model, which will affect the measured R_s values.

It is to be noted that, for diodes with thin epilayers and high doping concentrations (B22-21, B43-108), the series resistance increases with decreasing temperature. However, for diodes with thick epilayers and low doping concentrations (M45-116C, CTH 188.1), the series resistance increases with increasing temperature. This effect seems to be caused by the temperature dependence of the mobility, which for low doped GaAs is higher at 20 K than at 300 K.

The noise temperature versus bias current was measured at $f = 4$ GHz at test temperatures of 20 and 300 K with

Manuscript received January 29, 1985; revised April 17, 1986. This work was supported in part by the Swedish Board for Technical Development.

E. L. Kollberg and H. Zirath are with Chalmers University of Technology, Goteborg, Sweden.

A. Jelenski is with the University of Massachusetts, Amherst, MA 01003.

IEEE Log Number 8609250.

0018-9480/86/0900-0913$01.00 ©1986 IEEE

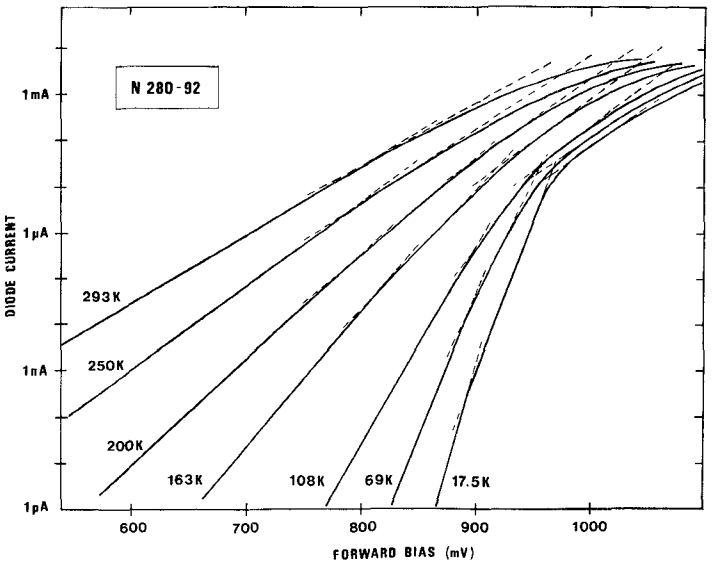

Fig. 2. Typical $I-V$ current–voltage characteristics of a Pt–GaAs junction for a temperature range from 17.5 to 300 K.

TABLE I
PHYSICAL AND ELECTRICAL DATA OF INVESTIGATED DATA

Diode	Anode metal	Diode[1] surface $S(\mu m^2)$	Epilayer thickness $d(A)$	Epilayer doping $N_d(cm^{-3})$	Breakdown volt. $V_{BR}(V)$	Zero Bias cap. $C_o(fF)$
N280-92 pt 27	Pt	11.1	1400	$3\cdot10^{16}$	6.9	11.4
B 22-21	Pt	6.5	1200	$2\cdot10^{17}$	6.5	8.6
CTH 188.1[2]	Pt	3.8	~3500	$2\cdot10^{16}$	17.5	3.4
2E1[4]	Pt	2.5	~1200	$4\cdot10^{16}$	7.5	–
M45-116C	Pt	28.3	25000	$6\cdot10^{16}$	>20	12.0
B43-108A	Pt	6.5	600	$5\cdot10^{16}$	4 0	13.1
A244-A55 [3]	Al	7.1	500	$1\cdot10^{14}$	5.5	14.5

1) Measured with a metallurgical microscope.
2) Diode processed by W. Kelly, Univ. of Cork, Ireland, on MBE material made by T. Andersson at Chalmers University of Technology.
3) The anode material is single crystalline aluminum on MBE material, produced by A. Y. Cho at AT&T Bell Labs.
4) Diode made by R. J. Mattauch, University of Virginia.

TABLE II
MEASURED AND CALCULATED DATA FOR DIFFERENT DIODES

Diode	Series resistance R_s Measured 300K Ω	Measured 20K Ω	Calculated 20K Ω	Estimated mobility 20K m^2/Vs	Electric field 20K,5mA (kV/cm)	Excess electron temp T_e Calculated (K)	20K,5mA Measured (K)
N280-92A	–	–	12 6	0.6	1.5	160	280
N280-92B	10.0	10.0	10.5	0.6	1.5	160	400
N280-92C	11.8	11.8	12.0	0.6	1.5	160	200
B 22-21	3.0	9.0	9 4	0.2	1.4	150	95
CTH-188.1	64.0	46	54.4	0.8	2.1[1]	450	600[1]
2E1	19.0	17.0	21.0	0.5	2.3[1]	320[1]	1000
M45-116-C	25.0	13.0	17.1	0.4	0.65	80	120
B43-108-A	7.9	9.0	–	0.5	2.3	155	250
A244-A55	10.0	10.0	–	0.3	1.22	100	80

1) At $I = 3$ mA (at 10 mA $T_e \gg 1000$ K).

the test apparatus shown schematically in Fig. 3. The expression utilized to determine the diode noise temperature T_D is also given in this figure. Fig. 4 shows the $\log I(V)$ and $T_D(I)$ characteristics for three different diodes on the same chip measured at 20 K. A correlation

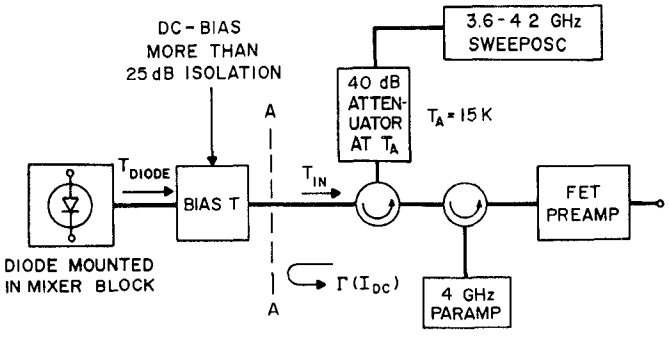

$$T_{IN} = T_{DIODE}\,(1-|\Gamma_D(I_{DC})|^2) + T_A\,|\Gamma_D(I_{DC})|^2 + T_{PARAMP} + T_{FET}/G_{PARAMP}$$

Fig. 3. Schematic diagram of the setup of 4-GHz noise measurement apparatus showing the diode connected to the bias T, circulator parametric amplifier, and FET preamplifier.

between the curvature of the $\log I(V)$ characteristic and the appearance of the excess noise, and big differences between diodes on the same chip can be seen. Fig. 5 shows the same curves measured at room temperature for one diode before and after exposing it to a short electric pulse, demonstrating the way in which similar and even more pronounced features, visible at high temperatures, can be obtained.

III. SCHOTTKY-DIODE PROPERTIES

A. The Classic log I(V) Characteristic

In this section, we discuss the $I-V$ characteristics expected from classical theories [6], [21] at ambient and cryogenic temperatures.

At temperatures above 100 K for typical diodes, the thermionic emission theory is said to describe well the current flow in metal–GaAs junctions giving

$$I = SA^*T^2\exp\left\{\frac{q(V-\phi_b-IR_s}{kT}\right\} \qquad (1)$$

where $A^* \simeq 8.2\times10^4 Am^{-2}K^{-2}$, T is the physical tempera-

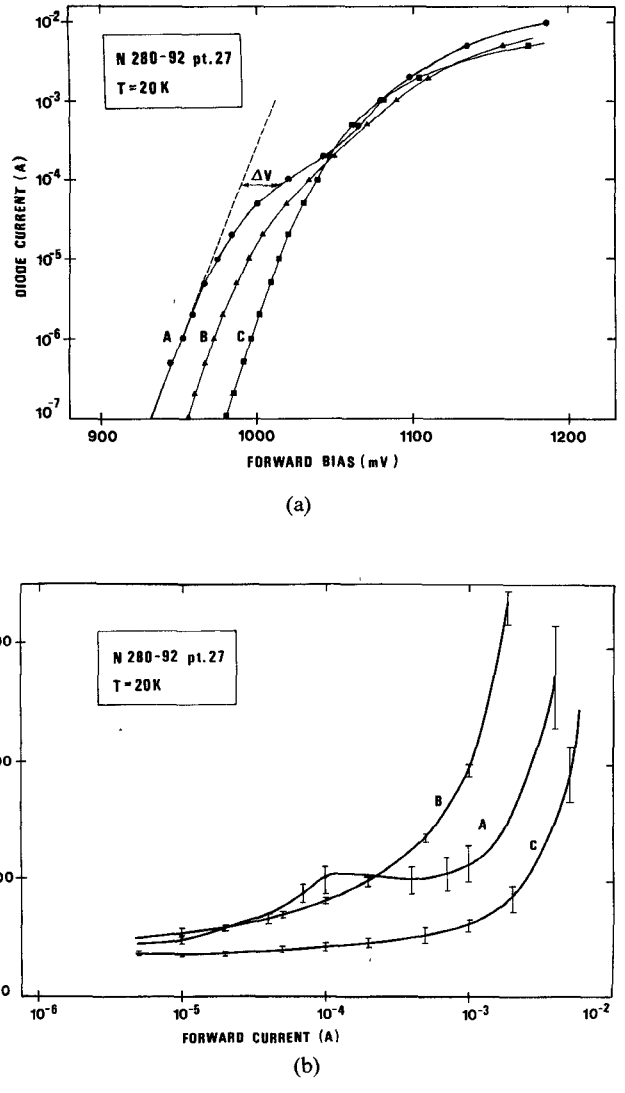

Fig. 4. Variations of diode characteristics across the chip. (a) The current–voltage characteristics of three diodes from the same chip. (b) The noise temperature as function of the forward current for the same diodes.

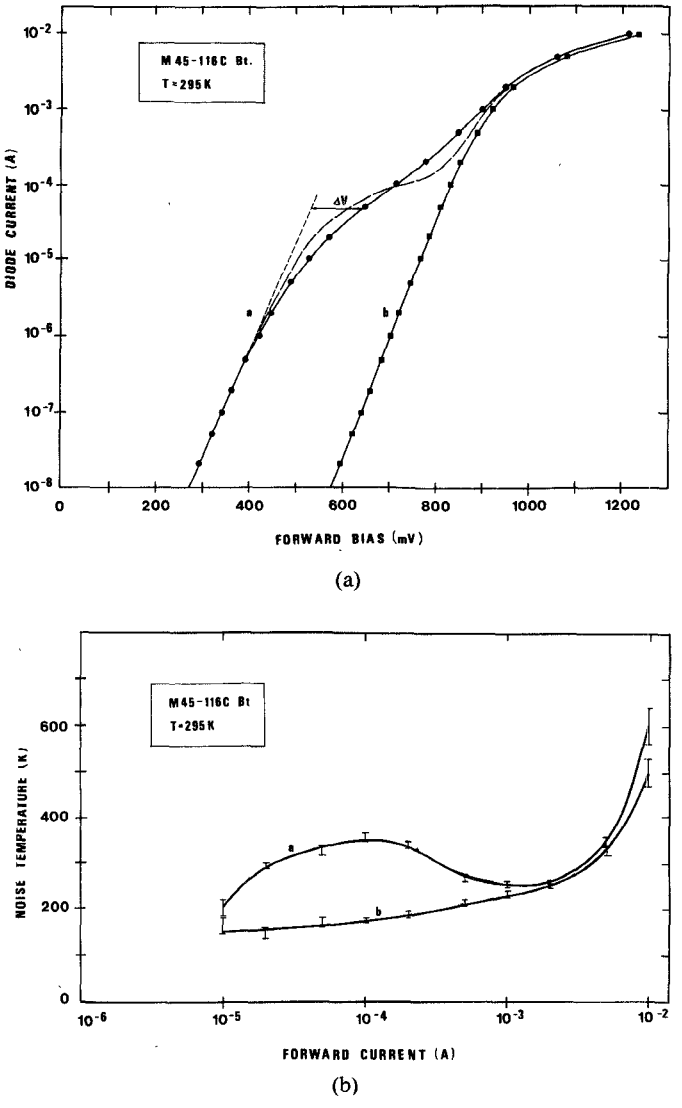

Fig. 5. The effect of a short electric pulse on diode characteristics. (a) Current–voltage characteristics (b) before and (a) after pulse. (b) Noise temperature–current characteristics (b) before and (a) after pulse.

ture, V is the applied voltage, ϕ_b is the barrier height which is slightly voltage and temperature dependent, S is the diode surface, and R_s is the diode series resistance. Often the value of the barrier height at zero voltage bias ϕ_{b0} is utilized, and the characteristic of a real diode is approximated by [21]

$$I = SA^*\theta^2 \exp \frac{q(V_j - \phi_{b0})}{k\theta} \tag{2}$$

where V_j is the barrier voltage $V_j = V - IR_s$. The "effective temperature" or "slope parameter" θ or an ideality factor $n = \theta/T$ of the diode is introduced to take into account any barrier-height voltage dependence, and contributions from transport mechanisms other than thermionic emission

$$\theta = n(V,T)T = \frac{q}{k}\frac{I}{dI/dV} = \frac{q}{k}IR_b. \tag{3}$$

The barrier differential resistance R_b can be calculated from (3). The barrier capacitance using a parallel-plate capacitance model is given by the expression [6]

$$C = \frac{C_0}{\left[1 - \dfrac{V_j}{\phi_b - V_n - \dfrac{kT}{q}}\right]^{\gamma}} \tag{4}$$

where C_0 is the diode capacitance at zero voltage $\gamma = 0.5$ for an ideal Schottky diode and qV_n is the energy difference between the bottom of the conduction band and the Fermi level shown in Fig. 1(b). (For $N_d = 3 \cdot 10^{16}\ \mathrm{cm}^{-3}$, $V_n \simeq 2$ mV at $T = 20$ K, and $V_n \simeq 75$ mV at $T = 300$ K.)

At low temperatures, the electrons do not have sufficient energy to pass over the barrier and can only tunnel through it. In the zero temperature limit, the current can be expressed as [14]

$$I = SA^*(\theta_F)^2 B \exp\left\{\frac{q(V_j - \phi_b)}{k\theta_F}\right\} \tag{5a}$$

where

$$B = \frac{1}{\ln\left|\frac{2q(\phi_b - V_j)}{\xi_2}\right|^2} \tag{5b}$$

$$\theta_F = \frac{q\hbar}{k}\sqrt{\frac{N_D}{4\epsilon m^*}} \tag{5c}$$

where N_D is the doping concentration, q is the electron charge, $\hbar$ is Planck's constant over 2π, k is the Boltzmann constant, ϵ is the dielectric permittivity of GaAs, m^* is the effective mass, and ξ_2 is the classical turning point energy at the slope of the barrier for electrons trying to pass through the barrier. The leading term B is difficult to determine, but it is approximately $0.3 \div 1$ for the investigated voltage range.

B. Device Properties Beyond the Classical Limit

In many current applications, Schottky diodes are driven into a current regime in which (2) and (5) are not more valid. This limit is reached if the built-in voltage V_{bi} shown in Fig. 1(b) becomes smaller than kT/q. An estimate of the critical current above which (2) and (5) are no longer valid is obtained by inserting into them V_j from the relation describing the so-called "flat-band" situation

$$V_{bi} = \phi_b - V_n - V_j = 0.$$

For example, one obtains for the diode N280-92 whose parameters are given in Table I a flat-band current $I_F = 1.4$ mA at $T = 20$ K and $I_F = 4.0$ mA at 300 K. These values are much lower than currents flowing at high forward bias and indicate that (2) and (5) cannot explain the observed $I-V$ characteristics in the full voltage range.

Another difficulty arises from the fact that the diode series resistance, which is caused by the undepleted epitaxial layer, is expected to be voltage dependent. It is to be noted also that the electron mobility and temperature become voltage dependent at high forward bias. Thus, the effective temperature θ in (2) will become voltage dependent.

As none of these parameters is directly measured, the evaluation of R_s in this high-current regime is quite difficult and the difference between the real and measured R_s values can be important.

Since typical millimeter-wave mixers and modulators work in this high-current regime during a part of the operation cycle, their behavior cannot be fully described by (2) or (5) and a constant series resistance. Moreover, it will be shown that even for currents much lower than the current corresponding to the flat-band, (2) and (5) cannot explain the experimental results. Some of the observed diode characteristics can be described only by the parallel diode model presented in Section IV.

C. Noise

At low current levels, the noise generated by Schottky-barrier diodes is caused by fluctuations of the number of electrons crossing the barrier (the shot noise) and their velocity fluctuations (the diffusion or thermal noise).

The shot noise temperature T_{sh} is directly related to the slope parameter of the $\log I(V)$ diode characteristic [13]

$$T_{sh} = \frac{\theta}{2} = \frac{1}{2}\frac{q}{k} I r_b \tag{6}$$

where r_b in this formula is the barrier differential resistance at the frequency of noise measurements. It can be lower than the value predicted from θ measured at dc if slow surface traps exist in the diode. In fact, some hysteresis effects were observed in some diodes.

The diffusion noise (which, in the investigated frequency range and for nondegenerate semiconductor material at low currents when the electrons are in equilibrium with the lattice, is equivalent to the thermal noise) can be described by the noise temperature equal to the ambient temperature T_0 [13].

At high current densities, other mechanisms are the source of a so-called "excess noise." They are voltage or current dependent and raise the diode noise temperature. The most important are intervalley scattering, carrier storage in traps, and hot electrons. The intervalley scattering occurs if the electric field in the epilayer is high enough to accelerate electrons to energies higher than 0.31 eV (necessary for their transfer to the upper valley in GaAs). This transfer eliminates the hottest electrons from the conduction band; however, since the transfer occurs with a certain probability, a new noise mechanism is added which is called intervalley scattering noise. This partition-type noise is white only for frequencies well below $f_{iv} = 1/2\pi\tau \simeq 90$ GHz, where τ is the lifetime in the upper valley of the conduction band in GaAs (1.8×10^{-12} s).

The presence of shallow traps in GaAs leads to a fluctuation of the number of electrons flowing through the diode, producing additional noise whose spectrum can extend even to microwave frequencies [33], [34], [38], [39]. If these traps are at the interface, they will affect the barrier height ϕ_b [21], the barrier resistance r_b, and cause a modulation-type noise, which adds directly to the shot noise. If the traps are in the undepleted epilayer, the noise will add to the intervalley scattering and hot-electron noise generated there. At frequencies comparable to the reciprocal value of the trap lifetime, this noise will strongly decrease, leveling off at lower and higher frequencies.

The hot-electron noise is generated in the nondepleted part of the epilayer if the electric field is high enough [16], [34]. Due to a nonlinear relationship between current, electric field, and electron temperature in this region, the results of Monte Carlo calculations [15] have been used to determine the hot-electron temperature T_h.

All the above sources of excess noise are current or electric field dependent and can be described by an excess noise temperature

$$T_e = \sum_n k_n(\omega) E^n \tag{7}$$

which can be compared to the expression derived by

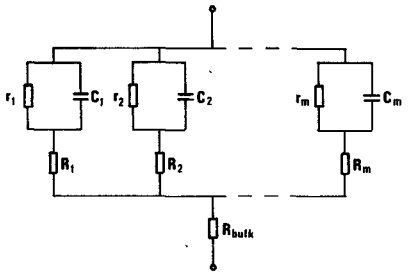

Fig. 6. Equivalent circuit of the parallel diode model for a metal–semiconductor junction.

Baechtold [34] for hot-electron and intervalley scattering noise in GaAs FET's.

Taking into account all noise sources described above, a formula for the measured noise temperature of a Schottky diode can be written as follows by extending the results derived in [13]:

$$T_D = \frac{r_b\theta/2 + r_s T_0 + r_{se} T_0\left(1 + \sum_n k_n I^n\right)}{r_b + r_s + r_{se}} \tag{8}$$

where r_s and r_{se} are substrate and epilayer resistances, respectively. At high frequencies, (8) should be modified to take into account the capacitance of the junction (see Fig. 6).

As in the case of $\log I(V)$ characteristics, this expression cannot generally explain the observed variations of noise temperature versus current (Fig. 4(b)) as it predicts a constant $T_D = \theta/2$ for low currents when $r_b \gg r_s + r_{se}$ and an increase of $T_D \simeq T_0(1+\Sigma_n k_n I^n)$ for high currents if $r_{se} \gg r_s$ and r_b.

IV. The Parallel Diode Model

The observed $\log I(V)$ and $T_n(I)$ characteristics for all measured diodes can be well explained by a model in which the diode is described as a sum of parallel metal–semiconductor junctions with different barrier heights ϕ_m, areas S_m, and series resistances R_{sm} (Fig. 6).

At low frequencies, subdiode capacitances C_{jn} can be neglected. Neglecting also substrate resistance r_s, one has

$$I = \sum_m I_m \tag{9}$$

$$T_D = \sum_m \frac{T_{d_m} g_m}{\sum_m g_m} \tag{10}$$

where I_m are currents flowing through particular subdiodes given by (2) or (5) with a proper barrier height ϕ_{bm}, $g_m = (r_{se} + r_b)_m^{-1}$ are subdiode conductances, and T_{d_m} are subdiode noise temperatures given by (8).

To make the model as simple as possible, a unique value of the slope parameter θ and of the epilayer conductivity was assumed for all subdiodes. It leads, at high currents, when r_{bm} can be neglected, to g_m proportional to subdiode area s_m.

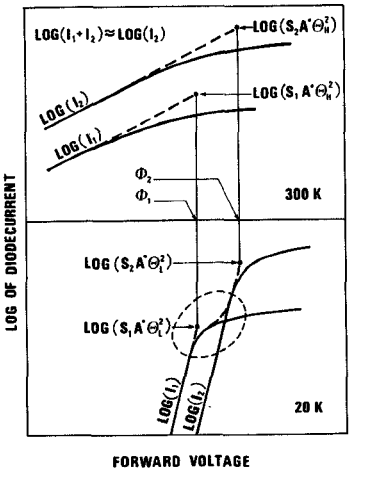

Fig. 7. Schematic drawing of the $I-V$ characteristics of a two-diode junction at 20 K and 300 K.

Subdiode junction capacitances c_{jm} can be calculated from (4) using $\gamma = 0.5$ and an appropriate value of ϕ_{bm} and S_m. Fig 7 illustrates why the effect of parallel diodes is more easily seen at low temperatures. The subdiode 1, which has a smaller area S_1 and barrier height ϕ_1, is driven to the flat-band at lower forward voltage, above which it acts simply as a resistance. Further increase of current is due to the parallel diode with a higher barrier height ϕ_2. This effect can be observed only if the slope of the $I-V$ curve is sufficiently high, i.e., at low temperature.

A computer program was utilized to find the appropriate subdiode parameters ϕ_{dm}, S_m, r_{bm}, r_{sem}. For moderate currents, it was sufficient to consider in (8) only the term corresponding to $n=1$. The comparison between measured and calculated current–voltage and noise characteristics for two diodes is given in Figs. 8 and 9, showing that this simple model gives a relatively good agreement even for the complex $\log I(V)$ and $T_D(I)$ curves shown in Fig. 9. The subdiode barrier heights obtained from this procedure for Pt–GaAs diodes are represented in Fig. 10, showing some characteristic values $\phi_{bn} \simeq 1.01$, 1.05, and 1.09 V at the temperature 20 K. Values of diode series resistance r_{se} calculated from the sum of g_m at high currents are also given in Table II (calculated). It can be seen from this table that the agreement between the two methods is satisfactory.

A possible explanation of this effect was given by Ohdomari and Tu [18] and Woodall and Freeouf [19], [20]. They assumed that microclusters of different compounds with different work functions are formed at the surface. Although Woodall and Freeouf describe the differences in barrier heights by different work functions of metallic compounds in microclusters (the Mott model of the diode [21]), similar effects can be obtained in the Bardeen model with different surface states and pinning energies for different compounds.

Different barrier heights of microclusters (subdiodes) in Pt–GaAs diodes can be caused by:

— locally Ga-rich or As-rich areas [22], [23] where metallic Ga or As and/or Ga_{As} and As_{Ga} antisities [24] can exist;

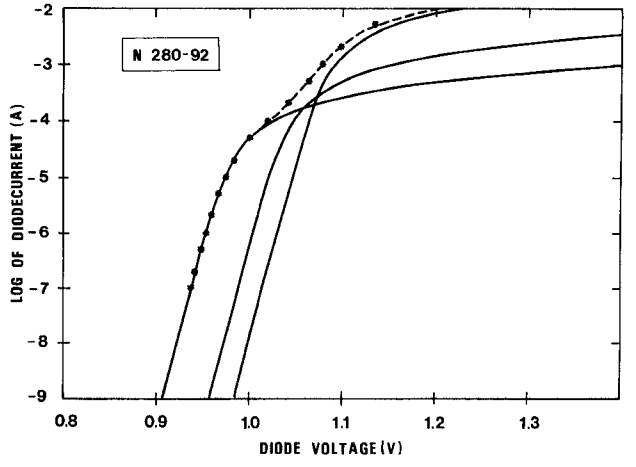

(a)

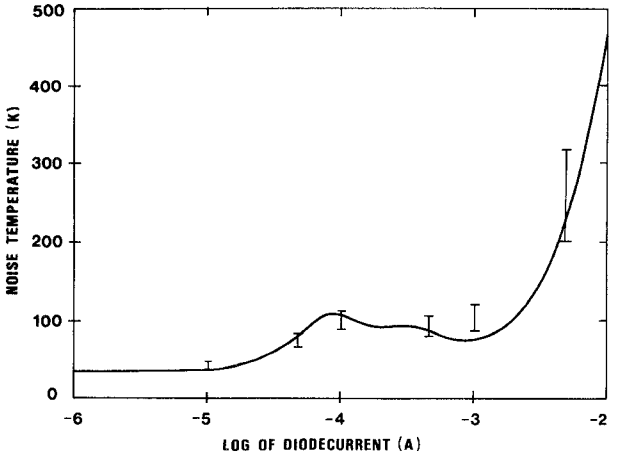

(b)

Fig. 8. Comparison between measured (points) and (a) simulated $I-V$ and (b) T_D-I characteristics assuming the existence of three subdiodes.

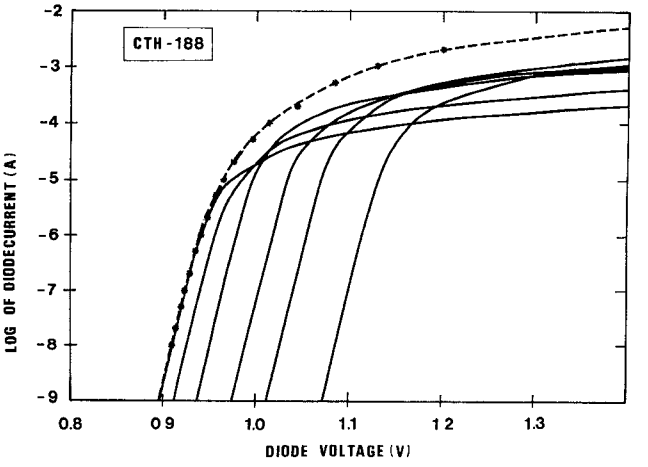

(a)

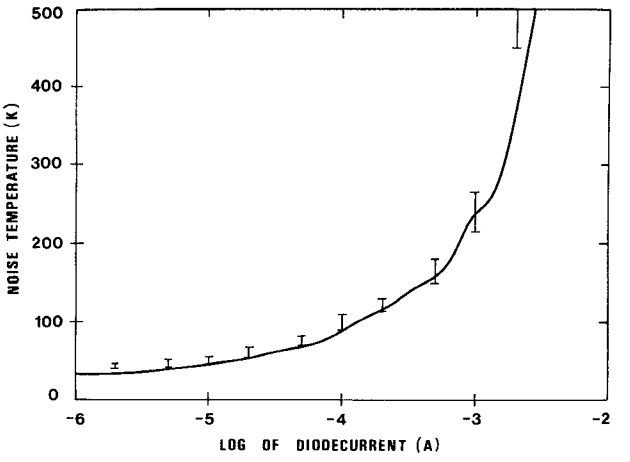

(b)

Fig. 9. Comparison between measured (points) and (a) simulated $I-V$ and (b) T_D-I characteristics assuming the existence of six subdiodes.

- the interdiffusion of Pt, Ga, and As [22] leading to the creation of clusters of different compositions such as $PtAs_2$ and Pt_3Ga [25]–[27];
- oxygen or oxide at the metal semiconductor interface [31];
- surface imperfection, exceeding metal particles, can lead to a barrier height decrease [28];
- local barrier height variation due to the pressure of the whisker, which can cause variations of the bandgap [29] or local changes of interface properties.

Despite the above arguments, other possibilities explaining the peculiarities in the observed $\log I(V)$ and noise temperature $T_D(I)$ dependence cannot be ruled out. One of them is the existence of traps close to the surface localized at discrete energy levels. These traps will produce variations of the barrier height and can be the source of additional noise as discussed above. Another possibility is the presence of trap levels emanating from the surface but penetrating some distance (~100–200 Å) into the epilayer [36]. They correspond to an initial higher doping of this region, which will decrease when these traps will be filled with electrons, leading to a decreased slope of the $\log I(V)$ characteristic. Of course, these traps can be localized in small areas, being the origin of subdiodes and clusters.

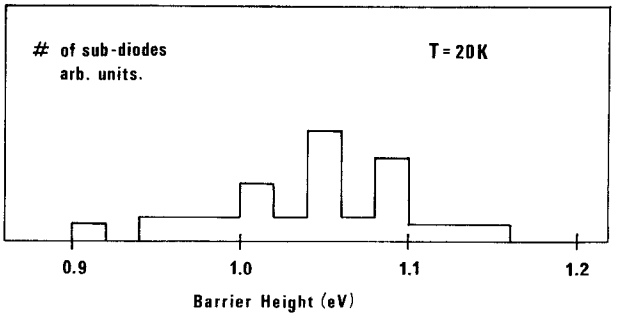

Fig. 10. The number of subdiodes versus their barrier heights, as measured at 20 K.

It is also possible that the whisker pressure on part of a diode surface can lead to subdiode creation. However, some pointing experiments performed did not confirm its importance.

V. Discussion

Fig. 11(a) shows the slope parameter θ, temperature-dependence curves derived from $\log I(V)$ characteristics as presented in Fig. 2 for two diodes (N280-92 and CTH

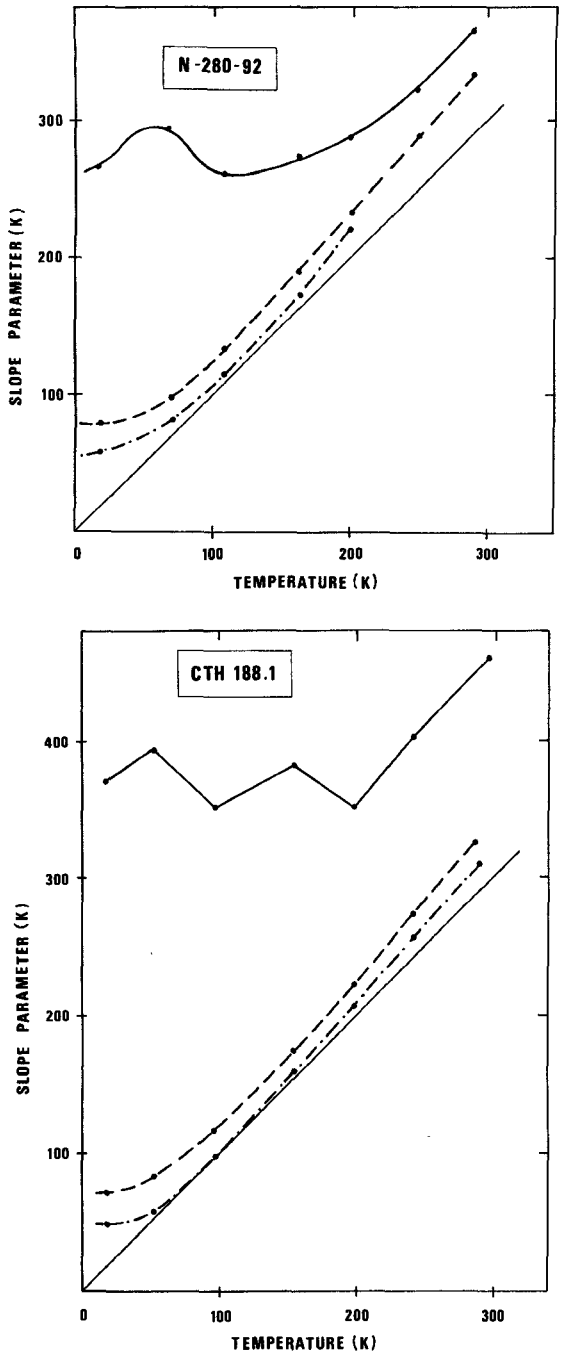

Fig. 11. Measured values of the slope parameter θ as function of temperature at current levels of 100 pA, 100 μA, and 1 mA, respectively, for two diodes.

188.1) with a thin and thick epilayer, respectively, for three different values of diode current. Each individual curve shows that the current is dependent upon the field emission at low temperatures, thermionic field emission, and thermionic emission at high temperatures [14]. However, for higher currents, $\theta(T)$ curves are shifted to higher θ values in contradiction to existing theory [13] predicting only one value. The possible explanations of this effect are: the barrier height variation with voltage due to an interfacial layer [21], electron heating [15], traps, and micro-clusters. The first two effects give a smooth θ variation with bias. All "knees" on the $I-V$ characteristic should be due to clusters or traps.

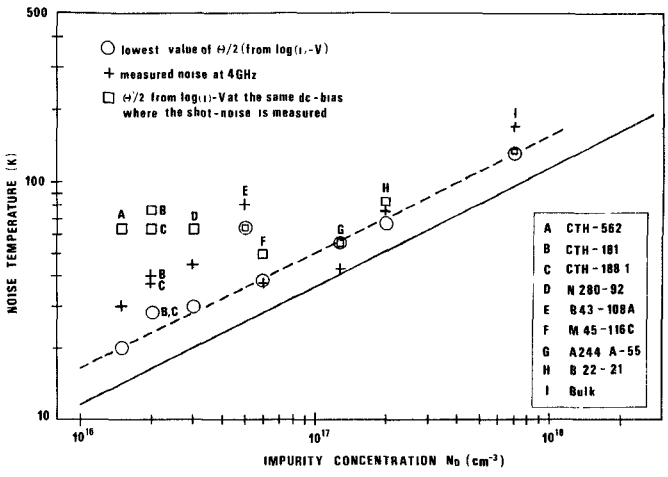

Fig. 12. Comparison of calculated and measured values of $\theta/2 = T_D$ as function of the concentration of the epitaxial layer.

A. The Low-Current Regime

At high temperatures ($\geqslant T = 100$ K) and for small current densities ($I \simeq 1$ pA), diodes are nearly ideal with $\theta = T$ as expected from thermionic emission theory. (See the lowest curve on Fig. 11.)

At low temperatures, field emission dominates but, even at low currents, the measured θ is higher than that predicted from (5c). It can be seen from Fig. 12, in which $\theta/2$ values obtained from (5c) (solid line), $\log I(V)$ measurements for very low currents (~ -100 pA) (circles) and noise temperature measurements at such low currents that hot electrons are not created (crosses) are compared. For most diodes, the lowest measured $\theta_m \simeq 1.4\ \theta_F$ (θ_F is given by (5c)). This result suggests that, for depletion layers of the order of a few hundreds angstroms, to determine θ, an effective N_d higher than the nominal concentration has to be taken. This higher effective N_d can probably be explained by the statistical distribution of the ionized dopants. With the diode current driven by regions with higher N_d, the effective N_d will be higher than predicted for a continuously distributed charge, leading to a higher effective θ as seen from measurements. For diodes with lower dopings, θ is also bias dependent as the measured θ values at greater currents ($\sim 10\ \mu$A) are much higher than predicted. (See squares in Fig. 12.)

Figs. 8 and 9 show that the parallel diode model explains pretty well the anamalous T_n behavior and excess noise appearing at relatively low current levels. For the same low-doped diodes, the noise temperatures T_D exceed $\theta/2$ determined for very low currents but are smaller than $\theta/2$ determined for the same current at which they were measured. This behavior can also be explained by the existence of relatively slow traps at the interface which do not contribute to the noise at 4 GHz.

B. The High-Current Regime

1) The slope parameter θ: Fig. 11 shows that, when the diode current increases, the horizontal part of the curve attributed to the field emission extends to higher temperatures and θ_F strongly increases. At sufficiently high ambient temperature, when thermionic emission should pre-

vail, the slope parameter can be expressed as

$$\theta = T_0 + \Delta T \tag{11}$$

with ΔT nearly independent upon temperature but increasing with the applied forward bias voltage (diode current). Such an effect can be caused by barrier lowering mechanisms in Schottky diodes. The image force lowering [21] for the considered diodes will have a negligible effect ($\Delta T \lesssim 3$ K) but the voltage dependence of the barrier height due to the existence of an interfacial layer $\gtrsim 10$ Å between the metal and the semiconductor gives a right order of magnitude of ΔT.

For high-current densities, the measured θ values will also be affected by the difficulties in the determination of R_s and its current dependence and by the increase of temperature of electrons arriving at the barrier, which can be seen from noise measurements, and which should decrease θ or both field and thermionic emission. Computer modeling is necessary to evaluate both influences.

Alternately, this effect can also be explained by the existence of subdiodes with different barrier heights carrying the current for different bias voltages. They can be caused, besides by the statistical donor distribution discussed above, by a similar effect concerning surface charges in the thin dipole layer at the metal–semiconductor interface. About 10^{12} electrons/cm^2 are required for creating a potential barrier of 2 V, which means that the "average" distance between charges is of the order of 100 Å. The statistical spread of these charges will cause the barrier height to be different from place to place. This second-order effect added to various mechanisms being the origin of subdiode barrier heights can lead to a statistical distribution of parallel diodes with slightly different barrier heights within each subdiode. In Fig. 13, the $\log I(V)$ characteristic resulting from a summation of equal area parallel diodes with different barrier heights is shown. The resulting $\log I(V)$ characteristic can be described by an effective θ much larger than θ of the individual diodes, and can explain large θ values observed for all examined diodes in the temperature range from 20–300 K at high current densities near flat-band.

C. The Barrier Height

For some diodes, subdiode features in the $\log I$–V characteristic (see, e.g., Fig. 2) are traceable over a large range of temperatures. Fig. 14 shows some typical plots of barrier height versus temperature obtained from measured "knee" voltages of the I–V characteristic and from the voltage drop on the diode above flat-band, assuming a constant R_s value. It is interesting to note that the barrier height decreases about 80 mV for a temperature change from 20 K to 300 K, close to the value of 70 mV calculated assuming that the ratio of the barrier height to the GaAs bandgap does not change.

It is also interesting to compare the most frequently measured subdiode barrier heights around 1090, 1050, and 1010 at 20 K (Fig. 10), which correspond to about 1010, 970, and 930 mV at 300 K, with earlier published data.

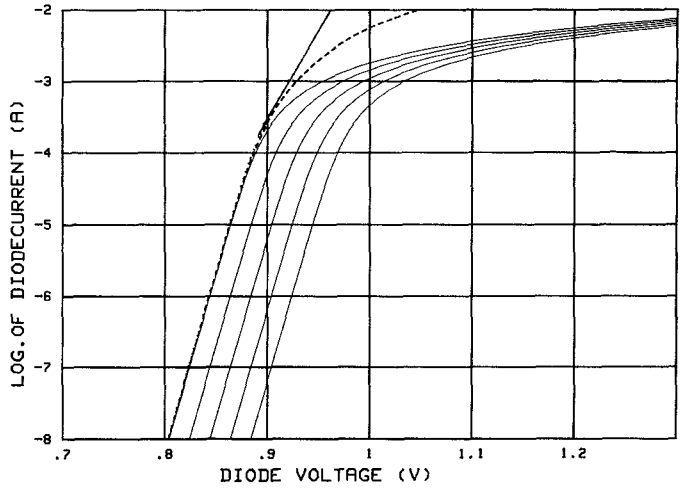

Fig. 13. Calculated current–voltage characteristic of a diode consisting of five subdiodes with equal areas.

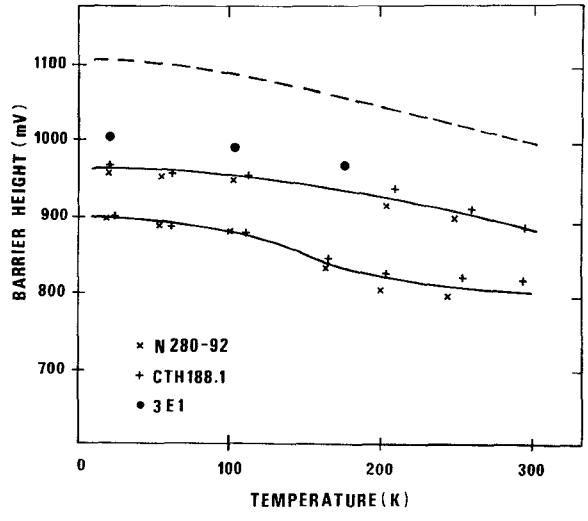

Fig. 14. Temperature dependence of the barrier heights evaluated from the "knee" voltages (points), and from the voltage drop corresponding to a constant current for an above flat-band operation of the N280-92 diode (----).

Sinha *et al.* [25], utilizing a CV technique, measured $\phi_b = 930$ mV for as-prepared diodes and 980 mV for diodes with $PtAs_2$ and Pt_3Ga complexes. The $C(V)$ measurements give approximately the barrier height at the flat-band ϕ_b^0 [21], and, as was pointed out by Ohdomari [18], they give the barrier height of the subdiode having the largest area even if this subdiode has the highest barrier height. Therefore, these values have to be compared with ϕ_b^0 estimated from observed "knee" voltages rather than with barrier heights at $V = 0$ obtained from $\log I(V)$ measurements, which according to [22] gives 780 mV for an As-rich surface and 870 mV for a Ga-rich surface. The above comparison of obtained data with Sinha results indicates that there is a strong probability that different compounds at the interface are the origin of at least some of the subdiodes.

1) The excess noise: Figs. 4(b) and 5(b) show that for sufficiently high current densities in subdiodes, an excess noise is generated. The corresponding electric fields have

been estimated from the relation

$$E = \frac{i}{qS\mu N_d} \tag{12}$$

valid for relatively low currents (μ is the low field mobility). The electron temperature was estimated from the curves $T_e(E)$ given in [15]. The resulting values are given in Table II. It can be seen that hot-electron noise is causing the major part of excess noise for these diodes.

For some diodes, the excess noise is considerably greater than the predicted hot-electron noise even for electric fields lower than the field at which intervalley scattering becomes important. It may be related to hot-electron noise of some subdiodes, carrying a substantial part of current or to some shallow traps in the epilayer or at the interface [39]. This noise would be frequency dependent and such a dependence was confirmed by N. Keen and the authors [32], [33], [40], [41], who found that the excess noise decreases strongly at frequencies between 1 GHz and 10 GHz at room temperature.

In CTH 188.1 and 2E1 diodes, extremely high noise temperatures (35 000 and 5000 K) were measured at 10 mA. As this current for these diodes corresponds to E > 4 kV/cm, where the intervalley scattering becomes important, all three sources of the excess noise seem to contribute. It is interesting to note that for the CTH 188.1 diode, the ratio of noise temperatures at 10 and 5 mA is 35 000/3900 in approximate agreement to the third power law quoted by Baechtold [34].

The third group of diodes exhibit a lower noise temperature than predicted. Two of these diodes have very thin epilayers (B-43, A-244), and some ballistic effects in these can be expected (see, for example, Shur [35]), but a more precise evaluation of the electric field in the epilayer has to be performed before such assignment can be made.

VI. Conclusions

It was found that electrical properties of Pt–GaAs microjunctions used as mixer diodes in cooled millimeter-wave mixers, which cannot be explained by one ideal Schottky-barrier diode in series with a resistance, are successfully described by a parallel diode model. Obtained results show the temperature and bias dependance of the barrier height, the slope parameter θ, and the noise temperature. These results seem to indicate that both clusters of different compounds and traps can be found in such diodes.

The low-temperature measurements of $\log I(V)$ and noise characteristics are a useful tool not only in studies of physical properties of Schottky microjunctions but also in predicting mixer noise performances and reliability.

Acknowledgment

The authors are indebted to Dr. M. V. Schneider for his assistance and for supplying them with diodes. They would also like to acknowledge C. O. Linstrom for his help during the measurements, and W. Kelly and T. Andersson, who processed some of the utilized diodes and epilayers.

References

[1] M. V. Schneider, R. A. Linke, and A. Y. Cho, "Low-noise millimeter-wave diodes prepared by molecular beam epitaxy (MBE)," *Appl. Phys. Lett.*, vol. 31, pp. 219–221, 1977.

[2] N. J. Keen, "Very low noise mixer at 115 GHz using a Mott diode cooled to 20 K," *Electron Lett.*, vol. 14, pp. 825–826, Dec. 1978.

[3] J. W. Archer, "All solid state low-noise receivers for 210–240 GHz," *IEEE Trans. Microwave Theory Tech.*, vol. MTT-30, pp. 1247–1252, 1982.

[4] D. N. Held and A. R. Kerr, "Conversion loss and noise of microwave and millimeter-wave mixers: Part 1—Theory," *IEEE Trans. Microwave Theory Tech.*, vol. MTT-26, pp. 49–55, Feb. 1978.

[5] D. H. Held and A. R. Kerr, "Conversion loss and noise of microwave and millimeter-wave mixers: Part II—Experiment," *IEEE Trans. Microwave Theory Tech.*, vol. MTT-26, pp. 55–61, Feb. 1978.

[6] S. M. Sze, *Physics of semiconductor devices*. New York: Wiley, 1981.

[7] E. Kollberg and H. Zirath, "A cryogenic millimeter wave Schottky diode mixer," *IEEE Trans. Microwave Theory Tech.*, vol. MTT-31, pp. 230–235, 1983.

[8] A. O. Lehto and A. Räisänen, "Embedding impedance of a millimeter wave Schottky mixer: Scaled model measurements and computer simulations," *Int. J. Infrared and Millimeter Waves*, vol. 4, pp. 609–628, 1983.

[9] C. R. Predmore *et al.*, "A broad-band ultra-low-noise Schottky diode mixer receiver from 80–115 GHz," *IEEE Trans. Microwave Theory Tech.*, vol. MTT-32, pp. 498–507, 1983.

[10] H. Zirath and E. Kollberg, "Characteristics of metal–semiconductor junction for mm-wave mixers," presented at Seventh Int. Conf. on Infrared and Millimeter Waves, Marseille, 1983.

[11] M. V. Schneider, A. Y. Cho, E. Kollberg, and H. Zirath, "Characteristics of Schottky diodes with microcluster interface," *Appl. Phys. Lett.*, vol. 43, pp. 558–560, Sept. 1983.

[12] E. Kollberg, H. Zirath, M. V. Schneider, A. Y. Cho, and A. Jelenski, "Characteristics of millimeter-wave Schottky diodes with micro-cluster interface," in *Proc. 13th Eur. Microwave Conf.* (Nuremberg), 1985, pp. 561–566.

[13] T. J. Viola and R. J. Mattauch, "Unified theory of high-frequency noise in Schottky barriers," *J. Appl. Phys.*, vol. 44, pp. 2805–2808, 1973.

[14] F. A. Padovani and R. Stratton, "Field and thermionic-field emission in Schottky barriers," *Solid-State Electron.*, vol. 7, pp. 685–707, 1966.

[15] T. J. Maloney and J. Frey, "Transient and steady-state electron transport properties of GaAs and InP," *J. Appl. Phys.*, vol. 48, pp. 781–787, 1977.

[16] P. J. Price, "Fluctuations of hot electrons," in *Fluctuation Phenomena in Solids*, R. E. Burgess Ed. New York: Academic Press, 1965.

[17] R. Fauauemberque, J. Zimmermann, A. Kaszynski, and E. Constant, "Diffusion and power spectral density and correlation function of velocity fluctuation for electrons in Si and GaAs by Monte Carlo methods," *J. Appl. Phys.*, vol. 51, pp. 1065–1071, 1980.

[18] I. Ohdomari, K. N. Tu, "Parallel silicide contracts," *J. Appl. Phys.*, vol. 51, pp. 3735–3739, 1980.

[19] J. L. Freeouf and J. M. Woodall, "Schottky barriers: An effective work functions model," *Appl. Phys. Lett.*, vol. 39, pp. 727–729, 1981.

[20] J. M. Woodall and J. L. Freeouf, "Summary Abstract: Are they really Schottky barrier after all?" *J. Vac. Sci. Technol.*, vol. 21, pp. 274–276, 1982.

[21] E. H. Rhoderick, *Metal–Semiconductor Contacts* (Monographs in Electrical and Electronic Engineering). Oxford: Clarendon Press, 1980.

[22] A. Aydinli and R. J. Mattauch, "The effects of surface treatments on the Pt/n-GaAs Schottky interface," *Solid-State Electron.*, vol. 25, pp. 551–558, 1982.

[23] W. E. Spicer, I. Lindau, P. Skeath, C. Y. Su, and P. Chye, "Unified mechanism for Schottky-barrier formation and *IV–V* oxide interface states," *Phys. Rev. Lett.*, vol. 44, pp. 420–423, 1980.

[24] R. E. Allen and J. D. Dow, "Theory of GaAs-Oxide interface states," *Solid State Commun.*, vol. 45, pp. 379–381, 1983.

[25] A. K. Sinha, T. E. Smith, M. H. Read, and J M. Poate, "n-GaAs Schottky diodes metallized with Ti and Pt-Ti," *Solid-State Electron*, vol. 19, pp. 489–492, 1976.

[26] V. Kulmar, "Reaching of sputtered Pt films on GaAs," *J. Phys. Chem. Solids*, vol. 36, pp. 535–541, 1976.
[27] D. J. Coleman, W. R. Wisseman, and D. H. Shaur, "Reaction rates for Pt on GaAs," *Appl. Phys. Lett.*, vol. 24, pp. 355–357, 1974.
[28] L. A. Rudnitskii, E. N. Martynyuk, and A. I. Reznik, "Electron work function of a nonideal metal surface III: Size dependence of the work function of a small particles," *Sov. Phys. Tech. Phys.*, vol. 27, pp. 711–715, 1982.
[29] V. L. Rideout, "Pressure sensitivity of gold-potassium tantalate Schottky barrier diodes," *Appl. Phys. Lett.*, vol. 10, pp. 329–332, 1967.
[30] D. E. Aspnes and A. Heller, "Barrier height and leakage reduction in n GaAs-platinum group metal Schottky barriers upon exposure to hydrogen," *J. Vac. Sci. Technol.*, vol. B1, pp. 602–607, July–Sept. 1983.
[31] C. M. Garner, C. Yu, W. Saperstein, K. Jew, C. Lee, G. Pearson, and W. Spicer, "Effect of GaAs or $Ga_xAl_{1-x}As$ oxide composition on Schottky barrier," *J. Appl. Phys.*, vol. 50, pp. 3376–3380, Mar. 1979.
[32] N. J. Keen, "Low noise millimeter-wave mixer diodes: Results and evaluation of a test program," *Proc. IEEE*, vol. A-27, pt. 1, Aug. 1980.
[33] N. J. Keen and H. Zirath, "Hot-electron generation in Gallium–Arsenide–Schottky-barrier diodes," *Electron. Lett.*, vol. 19, pp. 853–854, 1983.
[34] W. Baechtold, "Noise behavior of GaAs field-effect transistors with short gate lengths," *IEEE Trans. Electron Devices*, vol. ED-19, pp. 674–680, 1972.
[35] M. S. Shur and L. F. Eastman, "Near ballistic transport in GaAs devices at 77 K," *Solid-State Electron.*, vol. 24, pp. 11–15, 1981.
[36] J. Martinez, E. Calleja, and J. Piqueras, "Current/voltage characteristics of degenerated molybdenum and platinum Schottky diodes," *Electron. Lett.*, vol. 16, pp. 183–185, 1980.
[37] C. T. Sah, "Theory of low frequency generation noise in junction-gate field effect transistors," *Proc. IEEE*, pp. 795–814, July 1964.
[38] J. L. Pinsard *et al.*, "Microwave noise due to deep levels in GaAs MESFET's," in *Proc. Conf. on GaAs and Related Components* (Oiso, Japan), 1981, p. 431.
[39] G. N. Maracas, L. F. Eastman *et al.*, "Investigation of deep levels in GaAs MESFETs," in *Proc. 8th Biannual Cornell Engineering Conf.*, 1981, pp. 149–158.
[40] A. Jelenski, M. V. Schneider, A. Y. Cho, E. L. Kollberg, and H. Zirath, "Noise measurements and noise mechanisms in microwave mixer diodes," in *Proc. IEEE/MTT-S Int. Microwave Symp.*, (San Francisco, CA), May 1984, pp. 552–554.
[41] H. Zirath, S. Nilsen, E. Kollberg, T. Andersen, and W. Kelly, "Noise in microwave and millimeter-wave Pt-GaAs Schottky diodes," in *Proc. 14th Eur. Microwave Conf.* (Liege, Belgium), Sept. 1984.
[42] C. M. Wolfe and G. M. Stillman, "High purity GaAs," in *Proc. 3rd Int. Symp. GaAs, Inst. Phys. Soc. Conf.*, Ser. No. 9, pp. 3.
[43] I. Dimmock, "Hall coefficient factor for polar mode scattering in n type GaAs," *J. Phys. Chem. Solids*, vol. 31, pp. 1199–1204, 1970.

✠

Erik L. Kollberg (M'83–SM'83), photograph and biography unavailable at the time of publication.

✠

Herbert Zirath, photograph and biography unavailable at the time of publication.

✠

Andrzej Jelenski (M'84), photograph and biography unavailable at the time of publication.